ICAS 2016
30th Congress of the International Council of the Aeronautical Sciences
DCC, Daejeon, Korea : September 25-30, 2016

THE INFLUENCE OF A LOCAL CHANGE IN WING DIHEDRAL ON THE LOW SPEED FLOW CHARACTERISTICS OF RECTANGULAR PLANFORM WINGS

Kevin P. Garry, Jenny C. Holt, Geoffrey Tanguy, Simon A. Prince
Applied Aerodynamics Group, Cranfield University, UK

Keywords: *high aspect ratio, wing-fold*

Abstract

Aerodynamic load and flow field data, to support assessment of the possible use of in-flight activation of a chord-wise wing-fold as a gust alleviation device for a high aspect ratio wing, is obtained from a RANS CFD simulation and low speed wind tunnel measurements. The baseline configuration is a rectangular planform wing with a NACA 64(3)-418 section at a nominal Reynolds number (Re) of $1x10^6$ The wing incorporates a chord-wise fold line at 67% of the semi-span which allows the outer section to be set at a cant angle (ϕ) to the main wing of 15, 30 or 45 degrees.

Reductions in wing lift coefficient (C_L), lift-to-drag ratio and root bending moment were predicted with increasing wing cant angle. Incremental changes relative to the straight wing case were greatest at an incidence of nominally 10 degrees.

1 Introduction and Background

There is potential interest in the use of folding wings to facilitate ground operations of aircraft with high aspect ratio wings. It may therefore be possible to exploit the folding mechanism, which produces a local change in dihedral in the outer-wing span, as a means of active gust load alleviation for these wing configurations. There is relatively little published information available relating to the effect of local changes in dihedral in terms of the wing flow structure and overall aerodynamic loads. As a result, a coordinated programme of sub-scale wind tunnel tests, CFD simulations and analytical studies was undertaken, the primary objective being to understand variations in the flow structure, as a result of dihedral changes, particularly in the region of the wing hinge or fold-line. This data may be used to establish an active flow control strategy with potential application to a high aspect ratio UAV configuration. The focus is therefore on low Reynolds number applications, nominally $10^5 < Re_c < 10^6$ and simple un-swept, rectangular wing planforms.

2 Wing Configuration

The baseline wing configuration has a rectangular planform with a NACA 64(3)-418 section and chord (c) of 0.342m. The wing has a hinge/fold line located 1.45c in-board of the square-cut tip to enable the dihedral angle of the outer section to be set at 0 (straight case), 15, 30 and 45 degrees relative to the main wing, see Figure 1.

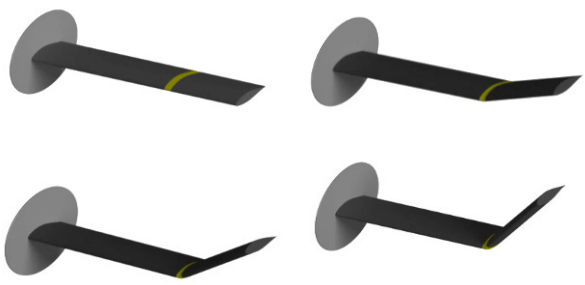

Figure 1. Schematic layout of the baseline rectangular planform wing with each of the tip dihedral conditions considered [7]

The inboard section is terminated by an elliptical end-plate in the wind tunnel model to aid simulation of an infinite semi-span. Various interchangeable inserts were used to investigate the impact of changes in the local geometry at the fold line.

2.1 CFD Simulation

The vertical and lateral extent of the computational domain was determined by that of the 8x6 wind tunnel working section, whilst extending axially 2m (5.8c) upstream and 8m (23.4c) downstream of the wing ¼ chord location.

The computational mesh was refined in the region of both the fold and the wing tip to facilitate capture of the detailed flow structure in these areas. The region around the end plate and its interaction with the wind tunnel working section ceiling was also detailed.

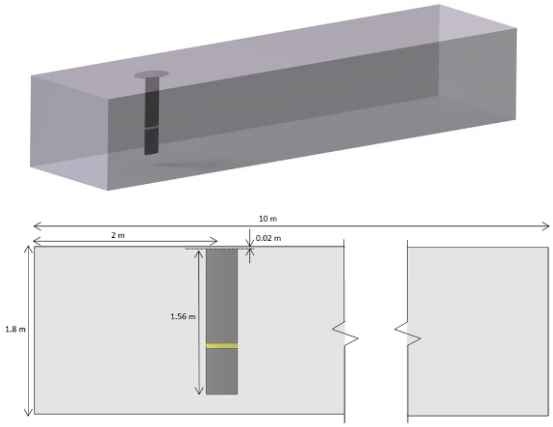

Figure 2. Arrangement of the computational domain reflecting the cross-sectional dimensions of the 8x6 low speed wind tunnel working section.

A summary of CFD boundary conditions is given in the table below.

Boundary	Type
Wing, Top, Bottom	Wall
Inlet	Inlet velocity
Outlet	Pressure outlet
Side	Inlet velocity

Table 1. A summary of the boundary conditions adopted in the CFD simulation.

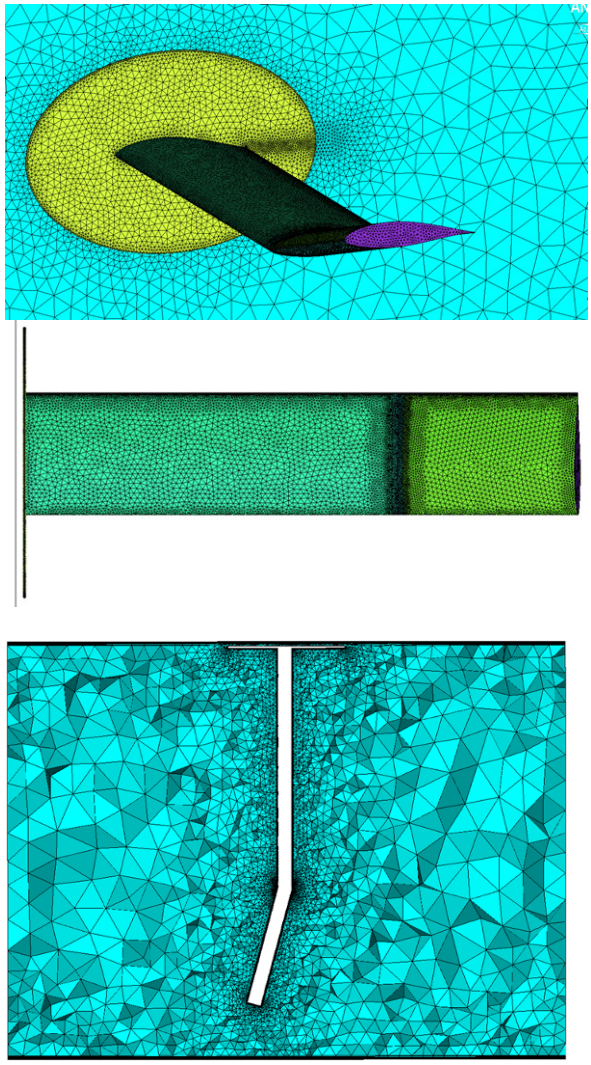

Figure 3. An illustration of the unstructured hybrid mesh used to used to establish the computational domain.

The simulations were run with a pressure based solver, the flow assumed to be incompressible, using the SIMPLEC scheme. Experimental data for validation purposes was taken from Render [6] who reported measurements on the original wing model, over a range of incidence angles, at a Reynolds number of $1x10^6$ (nominally 40m/s test section flow velocity at atmospheric conditions).

A number of alternative turbulence models were initially assessed against the experimental chord-wise pressure distribution taken from Render [6] for the incidence (α) = 3 degrees condition.

At low angle of attack the wing lift coefficient is underestimated for each of the turbulence models tested, see Tanguy [7] for

specific details. However, correlation with the measured drag coefficient was within 1% when using the k-ω STT turbulence model. This model has been previously shown to accurately simulate both near-wall regions and vortical flows, which makes it a suitable model to predict the forces and moments on the wing as well as areas of potential flow separation in the region of the wing-fold. The k-ω STT model was consequently adopted for the remaining numerical simulations, with a free stream turbulence intensity level of 0.1% (this corresponds to that measured in the 8x6 wind tunnel at 40m/s).

Analysis of the predicted lift coefficient (C_L) at Re = $1x10^6$ shows a clear effect of cant angle on both C_{Lmax} and lift-curve-slope at cant angles (ϕ) greater than 15 degrees, see Figure 4.

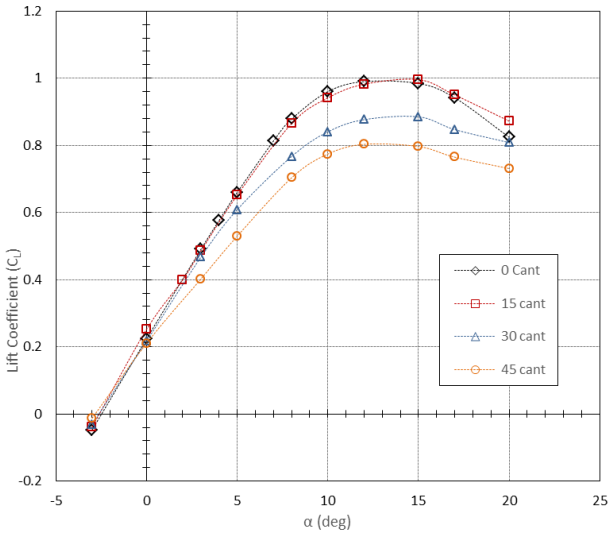

Figure 4. The effect of cant angle on the variation of lift coeffcient (C_L) with incidence (α) as predicted by the CFD simulation at Re = 1 x 10^6

The detrimental effect, as illustrated by the increment in C_L relative to the straight wing shown in Figure 5, is greater at the higher cant angle and peaks at wing incidence angles of nominally 10 degrees.

The wing maximum lift-to-drag ratio was reduced by 1.5%, 7.8% and 25.8% at cant angles of 15, 30 and 45 degrees respectively.

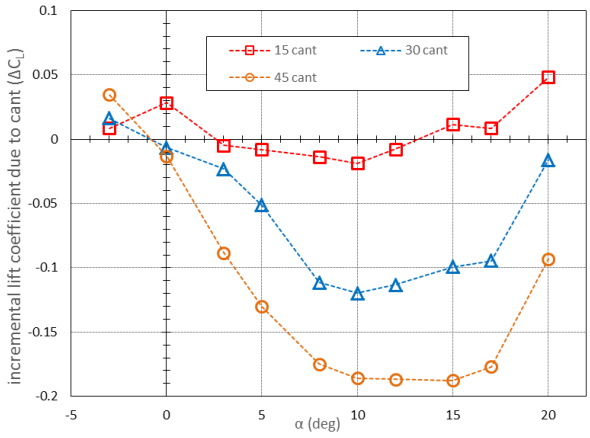

Figure 5. The effect of cant angle on the change in C_L, relative to the straight wing, as predicted by the CFD simulation at Re = 1 x 10^6

Increasing wing cant angle is seen to displace the span-wise centre of pressure in-board. The resulting reduction in the wing root bending moment coefficient, expressed as a percentage of the straight wing configuration at the same incidence, is given in Figure 6. The impact on wing root bending moment at 15 degrees cant angle is seen to be small but at 45 degrees cant angle the reduction is nominally 28%.

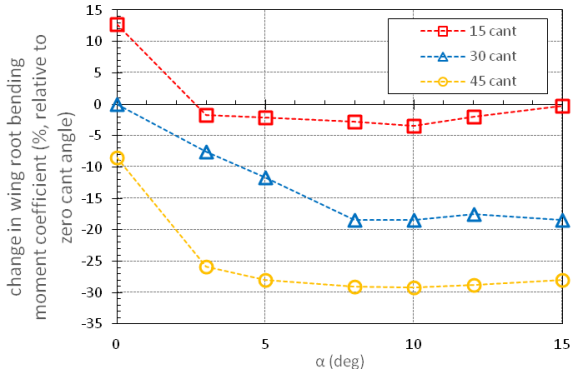

Figure 6. The predicted change in wing root bending moment coefficient with incidence (α) for each of the cant angles (Φ) tested, at Re = 1 x 10^6

An example of the wing-fold junction flow in terms of velocity contours taken from the CFD simulation at Re = $1x10^6$, at three wing cant angles with wing incidence (α) of 3 degrees, is given in Figure 7. The wing upper surface boundary layer is predicted to separate ahead of the trailing edge, at the spanwise

location of the fold. The separation point is seen to move forward with increasing cant angle and spreads rapidly spanwise – particularly for the $\phi = 45$ degree case.

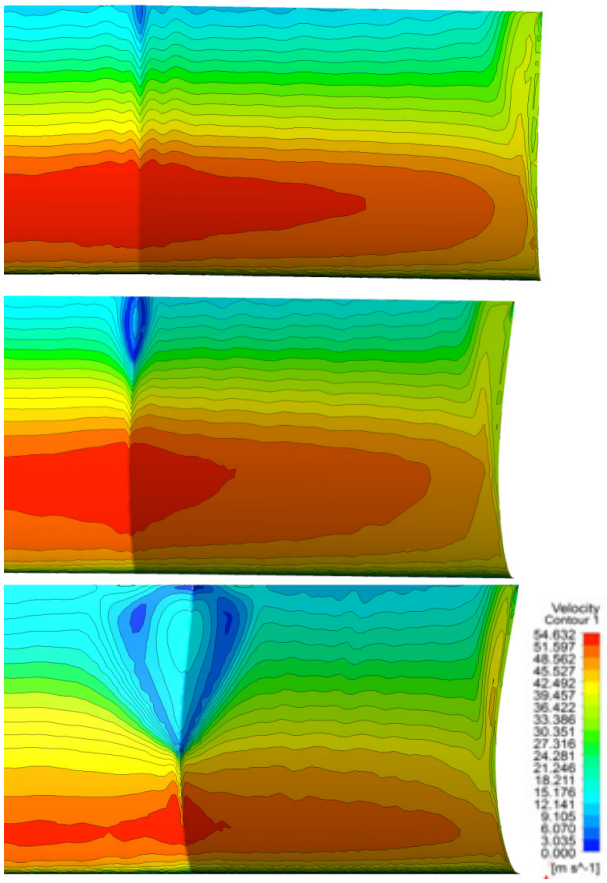

Figure 7. Surface velocity contours in the region of the wing fold at incidence 3 degrees, for cant angles (ϕ) 15, 30 and 45 degrees (top to bottom respectively).

Further analysis of the CFD simulation suggests that the region of flow separation near the fold, at ϕ=45 degrees, may be bounded by a horseshoe shaped vortex structure. This rolls-up rapidly in the wing wake to form a single vortex with the same sense of rotation to that of the adjacent wing tip vortex. It is recognized that the extent of this separation region for a given configuration and incidence, will depend on the detailed geometry of the wing at the fold line. In this case the junction was a simple extrapolation of the main wing and canted wing surfaces in order to establish a datum condition for possible further investigation with fairings etc.

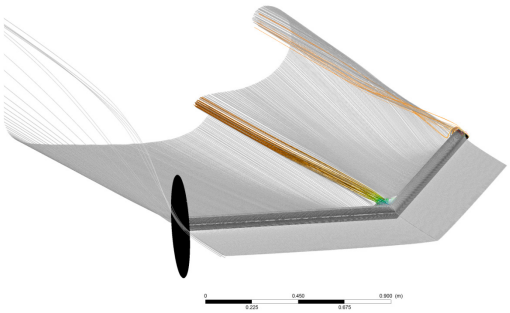

Figure 8. Streamlines illustrating the location and sense of ratation of the wing-fold vortex wake relative to that of the wing tip, incidence (α) = 3 degrees, wing cant angle (ϕ) = 45 degrees

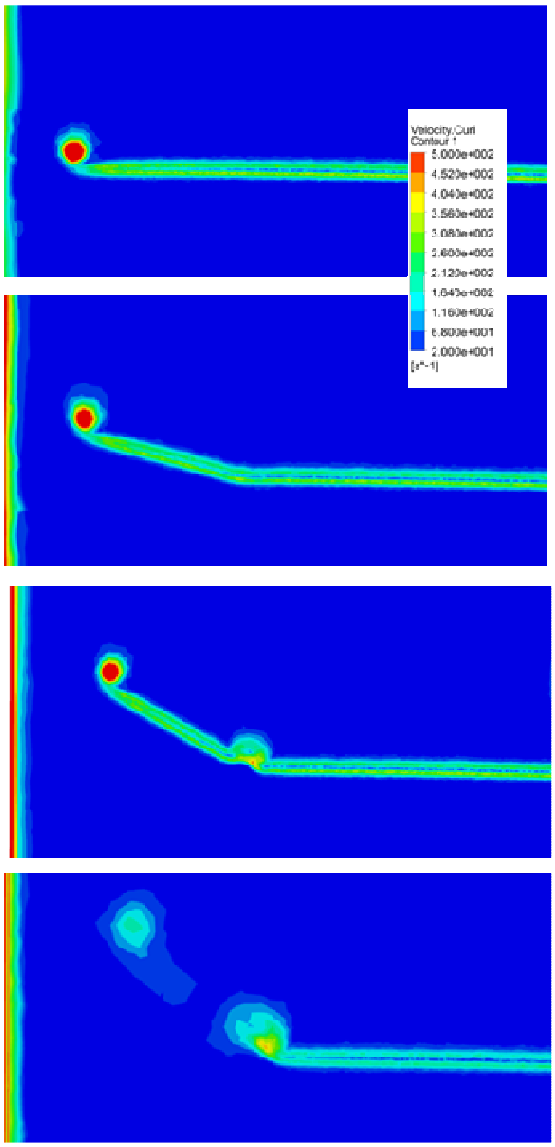

Figure 9. Contours of vorticity magnitude taken from the CFD simulation at Re = $1x10^6$ at incidence (α) = 5 degrees in a plane 0.5c downstream of trailing edge. Cant angles 0,15,30 and 45degrees (top to bottom)

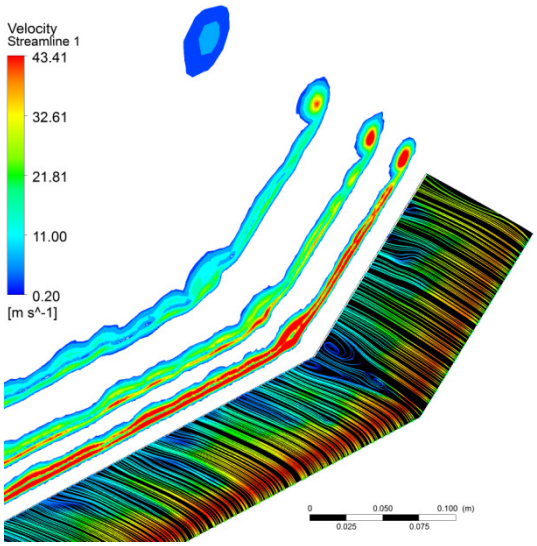

Figure 10. Velocity contours at incidence (α) = 6 degrees, cant angle (ϕ) = 45 degrees from the CFD simulation at Re = 1x10^6.

Figure 11. The baseline (zero cant angle) wing in the 8x6 wind tunnel working section (left) and an example of the foam inserts used at the fold-line to 'blend' the junction (right)

2.2 Experimental wake measurements

Experimental measurements are made to support the CFD simulation in the form of wake total pressure contours.

A rake of 40 total pressure tubes was traversed in a plane orthogonal to the wing trailing edge, 1 chord length downstream. Separation between the tubes was 4.7mm and the rake width nominally 20cms. Contours of local dynamic pressure were derived using the difference between the measured local total pressure and the static pressure taken from tappings in the wall of the test section at the corresponding axial location.

An example of the resulting contours in local dynamic pressure are shown in Figure 12 for a vertical plane downstream of both the wing tip and wing fold with a cant angle of 45 degrees. The trajectory of the vortical structures in the wing wake correlated with that predicted by the RANS CFD simulation at the same Reynolds number.

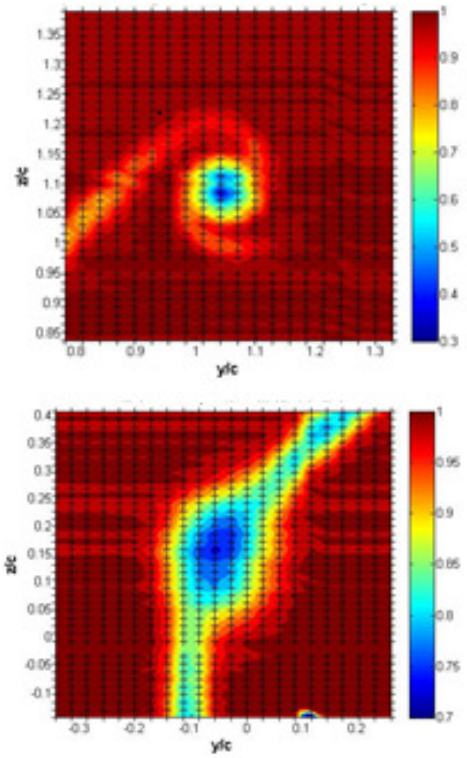

Figure 12. Examples of the normalised dynamic pressure contours measured in a plane 1 chord downstream of the wing trailing edge for the ϕ=45 deg configuration at α=5 deg

3 Conclusions

A RANS CFD simulation was used to assess the aerodynamic implications of a chord-wise 'fold' at 60% of the semi-span, on a rectangular planform wing with cant angles of 0 (straight case), 15, 30 and 45 degrees. Acceptable correlation with experimental data at Re = $1x10^6$ was achieved with a k-ω STT turbulence model using an unstructured hybrid mesh.

A detrimental effect on wing lift coefficient (C_L) and lift-curve-slope were seen, particularly at wing cant angles in the range $15<\phi<45$ degrees.

Corresponding maximum reductions of 25.8% and 28% in wing lift-to-drag ratio and wing root bending moment respectively were predicted.

Boundary layer separation at the fold location appeared to result in a longitudinal vortex, with the same sense of rotation as the wing tip vortex. CFD predictions of vorticity in planes downstream correlated the trajectory of the predicted vortical structure with contours of local dynamic pressure measured with a Pitot rake.

References

[1] Bourdin, P. Gatto, A. and Friswell, M.I. The application of variable cant angle winglets for morphing aircraft control. *AIAA 24th Applied Aerodynamics Conference* Paper 2006-3660 (2006).

[2] Gold N. and Visser K.D. Aerodynamic effects of local dihedral on a raked wingtip. *AIAA 40th Aerospace Sciences Meeting*, Paper AIAA-2002-0831 (2002).

[3] Jagannathan, R. *Experimental and CFD investigation of a high Aspect Ratio Wing with variable tip dihedral.* MSc Thesis Cranfield University (2014).

[4] Maan, G. *Experimental effects of wing tip geometry and sweep angle on wing tip vortices and transition for a high aspect ratio wing*. MSc Thesis Cranfield University (2014).

[5] Yen, S.C. and Fei, Y.F. Winglet dihedral effect on flow behavior and aerodynamic performance of NACA0012 wings. *Journal of Fluids Engineering*, Transactions of the ASME, 133(7) (2011).

[6] Render, P.M. *Aerofoil measurements at low Reynolds number.* PhD Thesis, Cranfield University UK (1984)

[7] Tanguy, G. *High aspect ratio wing with variable wingtip dihedral. Experimental and CFD investigation.* MSc.Thesis Cranfield University, UK (2014)

Contact Author Email Address

k.p.garry@cranfield.ac.uk

Copyright Statement